PHOENICS Newsletter

CHAM

Table of Contents

Spring 2024

Introduction

Bodies that move and vibrate or flex (e.g. fish, submersibles) in the density stratified depths of the ocean generate internal density waves. An earlier article in the PHOENICS Newsletter (Ref 1) explored 2-D oscillations of a body in a uniformly stratified environment.

This article extends the analysis to 3-D moving and flexing underwater bodies. When a 3-D body both moves and vibrates in a density stratified ocean, two waves systems are apparent, the internal waves due to the vibrating component (Ref 2) and the internal wave system due to the translating motion. PHOENICS is used to illustrate the analysis of this type of flow by using the ideas inherent in the MOFOR methodology for moving bodies (Ref 3).

Analysis

PHOENICS is used to solve the 3-D time dependent laminar equations of mass momentum and energy when a moving body flexes in a uniformly stratified environment. A Cartesian grid is used with the KOREN differencing scheme. The x, y and z coordinates are taken in the lateral and vertical directions respectively, with the x coordinate in the direction of translation and the z coordinate in the direction of oscillation. The local buoyancy frequency is given by

$$N = sqrt(-g \frac{\frac{d\rho}{dz}}{\rho})$$

where g is the acceleration due to gravity and ρ the density. For simplicity, a constant N is used for this analysis.

For a vibrating body, waves of frequency ω less than N (Ref 2) will be found in directions to the vertical, θ, where

$$\cos(\theta) = \frac{\omega}{N}$$

When a body is not translating but vibrating, the 3-D internal wave system lies on the boundary of a cone with apex centred on the body with apex angle 2θ (effectively revolving the 2-D wave system of Ref 1 about the z axis). There are various types of vertical vibration that can be analysed (Ref 1) but again for simplicity only a vertical sinusoidal oscillation will be considered in this article.

When a body moves horizontally in the x direction at constant speed a steady wave system is produced, centred on the body but extending from the body.

If the speed along the x axis is greater than the wave speed (the case considered here) the waves are swept back into a cone centred on the body so that a V-shaped wave pattern is produced in each horizontal plane (Ref 5).

For internal waves in a stratified fluid with constant N, a modal solution for the vertical velocity can be obtained consisting of horizontally travelling plane waves multiplied by a vertical sinusoidal eigenfunction of z. The corresponding dispersion relation (neglecting Coriolis effects) for the modes relating the plane wave frequency ω to the horizontal wavenumber, k, can then be obtained as (Ref 4)

$$\omega_n^2 = \frac{N^2 k^2 H^2}{k^2 H^2 + (n\pi)^2}$$

where n is the mode number ($1,2,3…$) and H the water depth. From this relation the mode wave phase and group speeds can be found as

$$C_p = \frac{\omega}{k} \quad , \quad C_g = \frac{\partial \omega}{\partial k}$$

Figure 1 shows the relation between ω and k and C_p and C_g for the first three modes for a water depth of $50m$ and N equal to $0.07rad/s$. In particular, mode 1 waves travel fastest and the phase speeds always exceed the group speeds (as expected) for each mode.
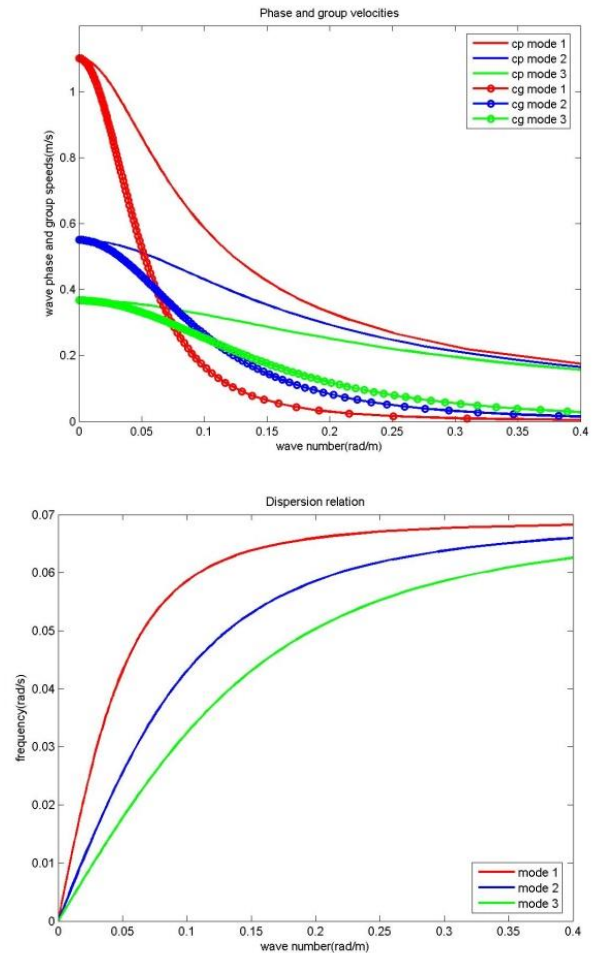

Figure 1. The top plot shows how the phase and group speeds vary with wavenumber for the first three modes. The bottom figure shows the relation between the wave frequency and wavenumber for the first three modes.

The steady, axisymmetric wave trajectories are then determined (for example in the x, y plane) as (Ref 5)

$$x = \frac{\varphi u (1 - \frac{C_p C_g}{u^2})}{k(C_p - C_g)} \quad , \quad y = \frac{\varphi C_g (1 - (\frac{C_P}{U})^2)^{\frac{1}{2}}}{k(C_p - C_g)}$$

Where u is the body speed in the x direction and ϕ is the wave phase. Figure 2 shows the calculated internal wave trajectories for the first three modes.
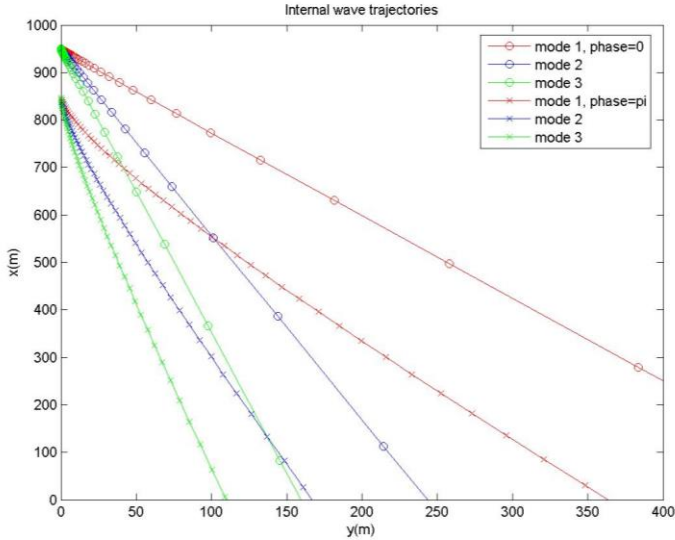

Figure 2. Internal wave trajectories for first three modes for phases of zero and π.

Three cases are considered. Each case considers a body moving at *2.2m/s* in a uniformly stratified fluid with *N* equal to *0.07rad/s*. Axial symmetry is exploited. Each case is run as a transient with the body starting from rest. In the first case the body is at *15m* depth, in the second at *25m* depth. For the third case the body at *25m* depth, vibrates vertically at a frequency of *0.035rad/s.*

Results

Figure 3 shows a typical run with the body moving along the x axis from right to left at *15m* depth.
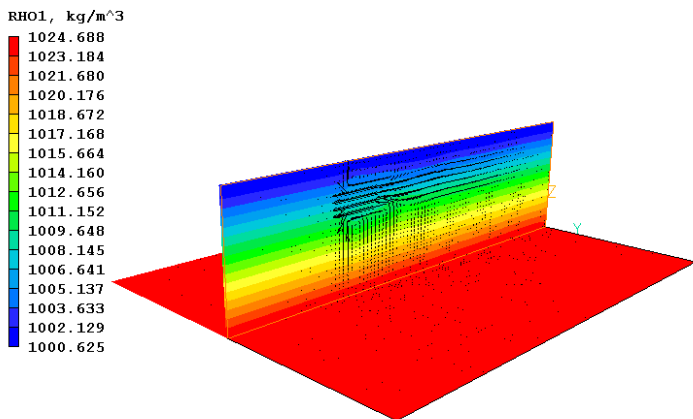

Figure 3. Velocity vectors for the MOFOR body at 15m depth moving from right to left in a uniformly stratified environment.

Different internal wave modes are stimulated when the body moves at different depths. With the body moving at *15m* depth, mode 1 waves are produced whereas when the body is moving at *25m* depth mode 2 waves are produced.

This is seen most easily by inspecting the contours of vertical velocity. Mode 1 waves have a single circulation in the vertical direction whereas mode 2 waves have a double circulation (a consequence of the sinusoidal eigenfunction solution). This is illustrated in Figure 4, as predicted by PHOENICS.
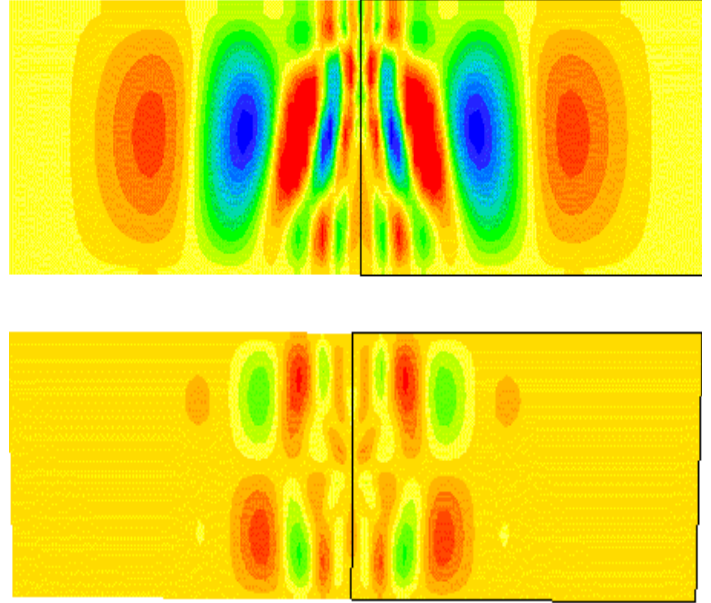

Figure 4. The top plot shows vertical velocity contours when the body is at 15m depth and the bottom plot when the body is at 25m depth. Note the single vertical circulation in the former case (mode 1 waves) and the double circulation in the latter case (mode 2 waves).

Internal wave profiles in a horizontal plane are shown most easily in contour plots of the *y* velocity.

Figure 5 shows comparisons of PHOENICS results for the surface wave profiles with the calculated trajectories for bodies at *15m* and *25m* depths. It can be seen that there is good agreement in both cases, for the former with the mode 1 trajectories and for the latter with the mode 2 trajectories (at zero and π phase).
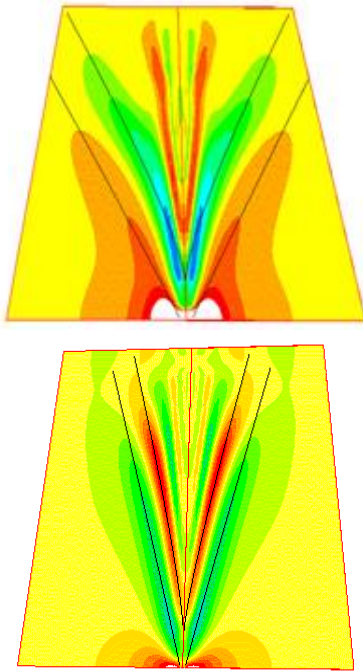
Figure 5. The top plot shows comparison of the PHOENICS internal wave surface trajectories with the calculated ones for a body at 15m depth (mode 1: lower black line phase zero and upper black line phase π). The bottom plot shows the equivalent comparison for a body at depth 25m (mode 2: lower black line phase zero and upper black line phase π). Note the greater wave speed of the mode 1 waves.

A third case where the body moves at *25m* depth but also oscillates vertically has been carried out. An initial inspection shows little difference between the cases with and without vibration. This is because the disturbance due to the translational motion is much larger than that due to the flexing action. Further cases are needed, where the body speed is reduced.

Conclusions

PHOENICS MOFOR results have been shown for a 3-D body moving at constant speed and depth in a uniformly stratified fluid. The results agree well with the calculated trajectories of the resulting internal waves and illustrate how different wave modes are stimulated by moving at different depths.

Results have also been obtained for the case when the body is flexing but these initially show that the relatively small flexing motion imposed is washed out by the waves generated by the larger translational motion.

References

1. Hornby R P. Internal Waves Generated by a Flexing Body. PHOENICS Newsletter Autumn 2023.
2. Lighthill M J. Waves in Fluids. Cambridge University Press 1978
3. Hornby R P. PHOENICS Modelling of a Moving Body in a Stratified Tank. PHOENICS Newsletter Winter 2019.
4. Apel J R. Principles of Ocean Physics, Academic Press 1995
5. Keller J B., Munk W H. Internal Wave Wakes of a Body Moving in a Stratified Fluid. The Physics of Fluids vol. 15, No. 6 p 1425-1431, June 1970

The term "Urban Heat Island" refers to a situation where a city or a built-up area has a higher temperature than the surrounding rural areas, due to the interaction of solar radiation with the hard surfaces of buildings and paved areas. In the context of CFD, an "Urban Heat Island" simulation often has a less specific meaning; it refers to the simulation of thermal effects in the built environment, possibly on a relatively small scale. In a typical commercial project a simulation might focus on a building or a group of buildings, together with their immediate environment; often the purpose might be to study pedestrian comfort in the spaces around a new development. A UHI simulation is typically a wind simulation with thermal effects added.

The thermal processes involved are complex. "Sunshine" consists of low-wavelength radiation; when this impinges on the ground or a building surface, the surface re-radiates with longer-wavelength thermal radiation.

As well as transferring heat to nearby surfaces, the latter is perceived by human beings as warmth, which can be measured by a variety of comfort indices available within FLAIR. Often, the purpose of a UHI simulation will be to determine how the distribution of a comfort index around a site changes in response to a new development. Typically, the comfort indices will be functions of parameters such as local temperature, radiant temperature, wind speed and humidity, and whether the person is in sun or shade.

We start with a typical simulation of wind flow around buildings, where the wind characteristics are defined using the Wind object in FLAIR. There is likely to be a "building of interest" modelled in detail with a fine mesh at the centre of the domain, with surrounding buildings modelled in less detail. Figure 1 shows the geometry and a typical mesh of a demonstration case for wind flow around a set of towers in a city in China.

Figure 1 – Mesh for typical wind case

The Sun object allows prescription of latitude, date and time of day, which determine the solar altitude and azimuth. Based on these data, FLAIR performs a shading calculation to determine which surfaces are sunlit (i.e. not in shade), and calculates the solar gain in W/m^2 on sunlit surfaces of buildings and the ground.

At all building and ground surfaces a surface heat-balance equation is solved. This contains the following terms, which are enforced to balance:

- thermal conduction in the ground or to the building interior (discussed below),
- solar gain – both direct and diffuse,
- re-radiation to other buildings, the ground or the sky,
- convective heat transfer to the wind,
- thermal capacity of the surface layer of the building or the ground.

The surface temperature appears in all the terms in the surface heat-balance equation, and so may be derived from this equation - it is stored in FLAIR as TWAL and can be inspected in the Viewer. Thermal re-radiation is solved using the IMMERSOL model in FLAIR.

A big question arises concerning how to model the thermal characteristics of the buildings. It would clearly be totally impractical to attempt to model the complete solid structure of each building; and representing buildings as homogeneous thermally conducting solids is very far from the reality. CHAM's recommended approach is to regard each building as having a shell of specified composition and thickness, with a temperature on the inside of this shell specified by the user, based on the typical temperature within the building. These parameters should all be entered in the Attributes dialog box for the building object, which should be created as a non-conducting Blockage (material 198). The "Energy Source" should be set to "Surface heat balance". Heat transfer through the shell is modelled as a conductive term in the surface heat-balance equation (see above).

Thermal effects in the ground may be treated in a similar way. The ground should be represented as a Blockage object, not a Plate – and so in the Wind object attributes, "Include ground plane" should be set to "No". A suitable thickness for the ground "shell" might be the depth below the ground surface at which there is no significant diurnal temperature variation. Temperature at this depth would need to be prescribed in the model. Alternatively, if the ground is flat, it may be meshed and modelled as a conducting material, so that "waves" of heat going into the ground in the day, and out at night, are modelled in detail.

The model should be run in transient mode, starting from a steady precursor solution for wind, through a number of day/night cycles until temperature predictions become periodic.

The model can handle the following effects.

- Direct and diffuse solar radiation on surfaces.
- Shading effects from buildings and trees.
- Radiant heat loss from urban fabric to the surroundings including the sky.
- Interchange of radiant heat between building surfaces, and between buildings and the ground.
- Effect of absorptivity / emissivity of surfaces.
- Thermal capacity in buildings and ground surface layers.
- Convective heat transfer to / from buildings.
- Effect on wind of trees / foliage.
- Evaporative cooling from greenery / foliage.
- Evaporative heat transfer from water surfaces or ground (crude model)

This is a complex topic, and modelling has the capability of becoming correspondingly complex. Our general advice would always be to commence by modelling a much-simplified system, and then (as necessary) increase the complexity of the model in stages, making sure that it works properly at each stage.

As an example, consider wind flow around the set of city towers shown above. The wind is 5 m/s at 10 m reference height, from the SW, with a logarithmic profile and a ground roughness height of 0.03 m. The wind temperature is 20 C. The case is very much a demonstration of capability; it has been run as a steady case with the solar gain reduced by a factor.

The sun settings correspond to the time 13.00 on 1 June, at 51 degrees latitude, with 1000W direct and 100W diffuse.The various constants in the model (emissivities, heat-transfer coefficients, sky temperature etc.) have been ascribed values which are reasonable but which should be researched in an actual study.
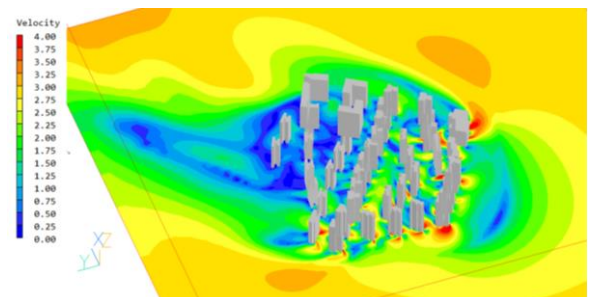

Figure 2 – Velocity contours 2m above the ground

Figure 2 shows velocity contours and vectors 2m above the ground, for wind around a set of city towers. The blue area towards the left shows the wake in the lee of the buildings.

Temperature variations at pedestrian level are very small, as seen in Figure 3.
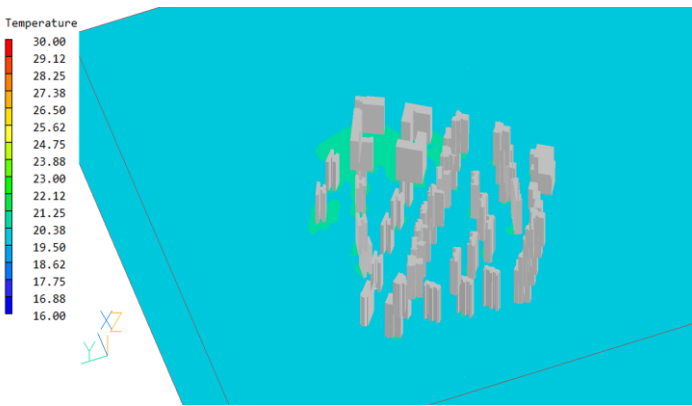
Figure 3 – Contours of temperature 2m above the ground

However, as Figure 4 shows, there is significant variation in the "Apparent temperature", a comfort index which is a function of temperature, radiant temperature and local air velocity.

This gives an indication of how a person would perceive temperature. Note how the building shadows are identified by the shading model, and are perceived to be cold regions; and the "warmer" area in the wake, where the wind velocity is reduced.
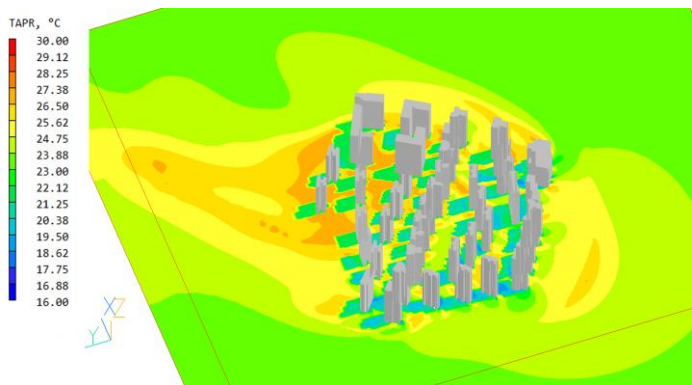

Figure 4 – Contours of apparent temperature 2m above the ground

Some of the parameters required for models of this type, such as heat-transfer coefficients and the sky temperature, are empirically based; and some features of the model carry considerable uncertainty, such as how best to implement an appropriate boundary condition for the ground surface. UHI models may need considerable tuning to perform at their best.

However, CFD always responds well to questions of the form – if input parameters are changed, what happens to the predictions? And so it will be here. CFD Urban Heat Island models will be an excellent tool to predict thermal changes in the environment following new building construction.

CHAM Support will be pleased to assist users who need advice concerning this interesting but complex application.

Numerical modelling of turbulent pipe flows of non-Newtonian fluids

Jorge Soto[1,2] and
Gianandrea Vittorio Messa[2]
Pontificia Universidad Católica de Chile[1]
Politecnico di Milano[2]

The importance of modeling turbulent flows of non-Newtonian fluids has increased due to the necessity of numerically simulating complex fluid dynamic processes in the extractive industry.

This industry produces large volumes of waste materials called tailings that exhibit rheological properties such as shear-thinning and yield stress.

Contrary to their Newtonian counterparts, the viscosity of these fluids continuously varies with the shear rate and fluctuates in turbulent conditions. Therefore, hydraulic transportation to the storage facility faces the challenge of accurately predicting the flow of such non-Newtonian fluids.

Computational Fluid Dynamics (CFD) codes offer several RANS models for Newtonian fluids which are very important for the design of transport systems.

For non-Newtonian fluids, the most common option is to solve the RANS for Newtonian fluids with a Reynolds-average viscosity dependent on the Reynolds average shear rate tensor; in non-Newtonian fluid mechanics, such models can be referred to as "Newtonian RANS models".

However, this is an approximate treatment of the non-Newtonian rheology, since the shear-dependent viscosity should be, in principle, decomposed into the average and the fluctuating components. Additionally, the fluctuating viscosity introduces new terms into the transport equations (Pinho, 2003).

While the contribution of these new terms can be very small when non-Newtonian properties are weak or the flow is highly turbulent, Newtonian RANS models tend to over predict the (average) viscosity in the region of low shear-rate for shear-thinning and yield stress fluids.

As part of his double PhD program between Pontificia Universidad Católica de Chile and Politecnico di Milano, the first author argued that limiting the maximum value of the average viscosity at low shear-rates can improve the estimation of the flow using Newtonian RANS models. PHOENICS has been utilised to develop the necessary modelling framework, and verify this assumption.

The attention was focused on turbulent pipe flows, which, in addition to being an engineering-relevant case study, allowed a throughout validation of the model by exploiting the many data available in the literature. In particular, the Direct Numerical Simulations (DNS) results of Singh et al. (2017, 2018) were used to evaluate the effect of shear-thinning and the Reynolds number.

For conditions beyond the DNS data, i.e., higher Reynolds numbers, the correlation of Dodge and Metzner (1959) and the expression proposed by Anbarlooei et al. (2015) were considered.

PHOENICS offers a variety of models suitable for simulating purely viscous non-Newtonian fluids, i.e., fluids that are inelastic and time independent. In particular, the two-parameter power-law rheology model is used to represent the shear-dependent viscosity of shear-thickening and shear-thinning fluids.

For shear-thinning fluids, the power law model predicts infinite viscosity in the limit of very low shear rate. Therefore, an additional third parameter is available to limit the maximum viscosity to a more realistic value.

In this work, the maximum viscosity is used to control the overestimation in the viscosity profile. The maximum viscosity is obtained from the power law model by considering a fraction of the shear rate found at the wall. It is selected to only affect the logarithmic layer and the core region

The flow is modeled as one-dimensional, axisymmetric, fully-developed, using the cylindrical-polar coordinate system. Therefore, the computational domain is represented by a single slab of cells in the axial direction, as shown in Fig. 1.

In the radial direction, the distribution of cells follows a geometric progression to ensure a high concentration of cells close to the wall. The eddy viscosity is calculated using three distinct low-Reynolds turbulence models: Lam-Bremhorst k-ε model, Two-layer k-ε model, and k-ω SST model. At the pipe axis, a zero-flux condition is employed for all variables.

At the pipe wall, the no-slip condition is set for the velocity, plus additional conditions associated with the selected turbulence model.

The numerical solution is obtained iteratively by using the PHOENICS single-slab solver (see Madhav and Malin (1997)) in the mode where the mean axial-pressure gradient is specified, and the mass flow rate is an outcome of the solution.
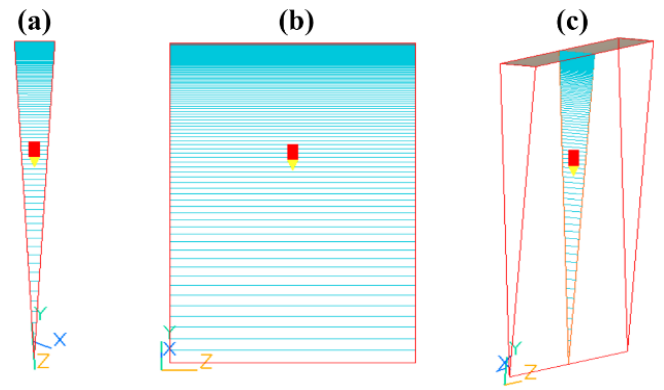

Figure 1. The discretization of a single slab of pipe: (a) front view, (b) side view and (c) diagonal view

By way of example, some results of the friction factor are shown in Fig. 2 for shear-thinning ($n < 1.0$), Newtonian ($n = 1.0$) and shear-thickening (n > 1.0) fluids. The curves on the left side show the estimation of the friction factor without any modification of the rheological model, whereas on the right side, the proposed limitation to the maximum viscosity was introduced.

It is observed that, for Lam-Bremhorst k-ε and Two-Layer k-ε turbulence models, prediction of the friction factor was improved for all shear-thinning fluids, and the error is reduced when the generalized Reynolds number is increased.

On the contrary, the solution of the k-ω SST turbulence model is almost insensitive to the limitation of the maximum viscosity. However, the k-ω SST turbulence model shows good prediction for weakly shear-thinning and shear-thickening fluids, and for high Reynolds number when $n = 0.6$.

The performance of k-ω SST turbulence model was also confirmed by Lovato et al. (2022). Additional effort will be directed towards the deeper understanding of the physical reasons which make the proposed methodology effective, thus making it conceptually stronger.

The analysis of the mean axial velocity profile, average viscosity, mean shear stress budget and turbulent kinetic energy will elucidate the effect of limiting the maximum viscosity.

Finally, the methodology will be further tested by considering other turbulence-modelling options to better assess its reliability.

Figure 2. Friction factors of power law fluids calculated with Lam Bremhorst k-ε (LB), Two Layer k-ε (2L), and k-ω SST (SST) turbulence models. The different models are compared before (left) and applying a limit to the maximum viscosity (right).

References

Anbarlooei, H. R., Cruz, D. O. A., Ramos, F., & Silva Freire, A. P. (2015). Phenomenological Blasius-type friction equation for turbulent power-law fluid flows. Physical Review E - Statistical, Nonlinear, and Soft Matter Physics, 92(6), 5–9. https://doi.org/10.1103/PhysRevE.92.063006

Dodge, D. W., & Metzner, A. B. (1959). Turbulent flow of non-newtonian systems. AIChE Journal, 5(2), 189–204. https://doi.org/10.1002/aic.690050214

Lovato, S., Keetels, G. H., Toxopeus, S. L., & Settels, J. W. (2022). An eddy-viscosity model for turbulent flows of Herschel–Bulkley fluids. Journal of Non-Newtonian Fluid Mechanics, 301, 104729. https://doi.org/10.1016/j.jnnfm.2021.104729

Madhav, M.T., Malin, M.R. (1997), The numerical simulation of fully-developed duct flows. Applied Mathematical Modelling, 21: 503-507, https://doi.org/10.1016/S0307-904X(97)00041-3.

Pinho, F. T. (2003). *A GNF framework for turbulent flow models of drag reducing fluids and proposal for a k − ε type closure*. *114*, 149–184. https://doi.org/10.1016/S0377-0257(03)00120-4

Singh, J., Rudman, M., & Blackburn, H. M. (2017). The influence of shear-dependent rheology on turbulent pipe flow. *Journal of Fluid Mechanics*, *822*, 848–879. https://doi.org/10.1017/jfm.2017.296

Singh, J., Rudman, M., & Blackburn, H. M. (2018). Reynolds number effects in pipe flow turbulence of generalized Newtonian fluids. *Physical Review Fluids*, *3*(9). https://doi.org/10.1103/PhysRevFluids.3.094607

Computational Prediction of COVID-19 Transmission in Internal Air-Conditioned Environments

I. Rentoumis, N.C. Markatos

CFD Unit, School of Chemical Engineering

National Technical University of Athens

Tel.: +30210772 3126.

E-mail address: n.markatos@ntua.gr

Abstract

COVID-19 has had destructive consequences for health and the economy and has altered every aspect of everyday human activity [1,2]. Public distancing in internal environments has been applied as a safety measure to prevent transmission. A controversial topic is the safe distance from person to person. The social distancing regulation, for internal public places, has been arbitrarily defined ignoring the potential aerodynamics effects of inlets, such as air-conditioning units, windows, and doors. The velocity of the intake airflow has the potential to transfer a droplet from the nose or the mouth of a patient in greater than the indicated distance.

The present study focuses on a model of a supermarket that includes a ventilation system and open doors.

For the transmission of COVID-19 in an air-conditioned internal space, two cases are investigated:
a) free flow and
b) louvre guided air flow.

Internal shelving, furnishing and human models are also being considered. The numerical results obtained are compared with those obtained by two well-known empirical models related to the effective velocity of incoming air and the virus concentration.

It is concluded that the computational results obtained in the present study are in acceptable agreement with those obtained by simple empirical models.

Finally, the PHOENICS mathematical model developed is flexible; and may be easily applied to any internal air-conditioned, environment or not, where many people meet (e.g. banks, retail shops, restaurants, etc.) to provide information and useful guidelines for social distancing in times of pandemia.
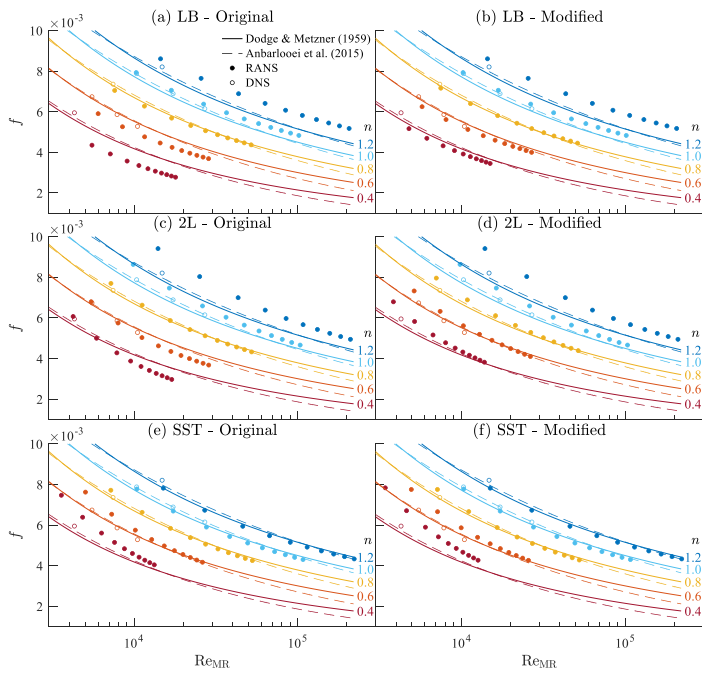
1. Introduction

Even though the transmission rate in China, the country of origin of COVID-19 has been brought down, there are several other countries around the globe that are struggling to contain the disease (Hossain Irin, 2020). Research has shown this disease to be transmitted though saliva, in the form of small droplets produced by sternutation and coughing (Xia Yanga, 2020). Therefore, there may be airborne infection due to pathogen matter in the form of small particles that disseminate the virus, spreading through large areas as aerosols (Public Health, 2020).Aerosols formed from persons infected with SARS-CoV-2 have the potential, under experimental circumstances, to remain viable and infectious for hours (Neeltje van Doremalen). Even though those tests were conducted at laboratory environments, there are enough to demonstrate the transmitting potential of the virus aerosols. Although different safe distance measures have been applied around the globe, the most common one is the 1.5m distance (C. Reinders Folmer M.E., 2020). Thus, it has been shown that the majority of droplets land on the ground, or they evaporate before reaching the distance of 1.5m.. Unfortunately, real internal environments that always include doors, windows, and other elements such as desks, chairs and various working units, all of which are altering the aerodynamic characteristics, have not been taken into account. Furthermore, the air-conditioning in most public spaces strongly affects the temperature stratification in the interior of a building (Dhakar, 2018).

The purpose of the present work is to test the validity of the simple empirical models and to provide a flexible prediction tool for more sophisticated guidelines concerning safe distances among people in public spaces of realistic configurations. The computational tool is demonstrated by applying it to a large, air-conditioned supermarket, for two design cases.

2. The problem considered, and modelling assumptions.

As an example of modelling a public place contaminated by a virus, a supermarket was chosen in two different designs. Design 1 is intended to simulate a large supermarket with many inlets and outlets. Two people have been placed with a distance of 1.5 m between them, facing each other. One of them is a virus carrier and the second human model acts as the receptor of the concentration level at 1.5 m. Design 2 is intended to simulate a smaller building with a more insulated environment, and there exists only one human model as 'patient zero'. Comparison can be made between the two models, as the first is centralized on a multivariable environment. On the contrary, design 2 has fewer inlets and outlets, and this may alter the result. Furthermore, the second human model is absent purposely, so that further

than 1.5 m distances can be researched. The supermarket consists of doors, ventilation on the ceiling, air-conditioning units on the two sides, stacks, a cash desk and two persons.

The assumptions made for the simulation approach are the following: (a) steady-state simulation of incompressible flow of a Newtonian fluid, (b) adiabatic walls, (c) constant air properties at 25.5°C, and (d) COVID-19 droplets have been modelled by their concentration in air.
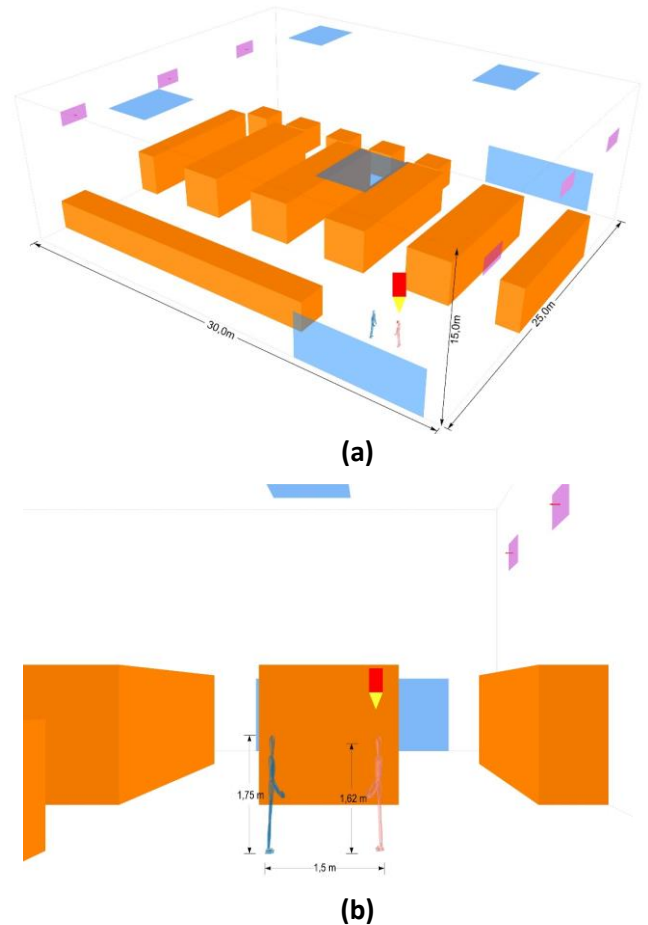

(a)

(b)

Figure 1 – Design 1: (a) overall internal geometry, (b) the human models
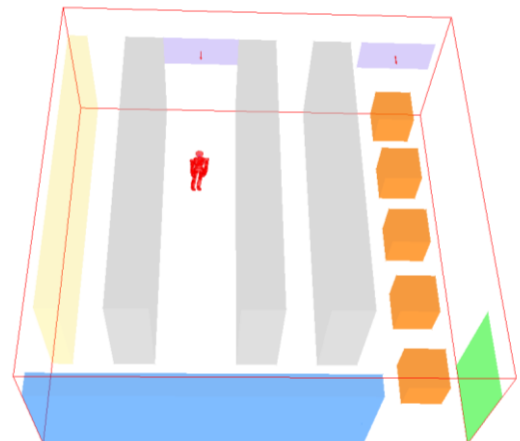

Figure 2 - Design 2: overall internal geometry

3. Mathematical modelling

The flow can be characterized using the three velocity components (u, v, w), pressure p, enthalpy, virus concentration, kinetic energy of turbulence, k, and its dissipation rate ε, as solved by the PHOENICS software [2019]. Most of the turbulence models in PHOENICS were used, but they gave similar results. More details may be found in literature, e.g. [4,7].

The solution domain of the first design has dimensions: X=25m, Y=25m and Z=10.5m and the A/C units were placed at 8 m height. To compare with a smaller domain, design 2 has smaller dimensions: X=10m, Y=10m and Z=4m and the A/C units were placed at 2,5 m height. The grid-sensitivity study indicated that the required grid was 1,357,752 cells.

The conditioned air is introduced in the supermarket as inlets having a constant velocity of 0.5 m/s. In the first design, six units are placed at 7.5 meters height. Three are placed in the plane Ymin and the other three in Ymax at 25 m.

The placement at X axis is 4.5, 11 and 17 m and is the same for the three at the opposite side of the room. In the second design, we have 2 units in the same side of the room, placed at 2.5 m in the Z axis and at 3 and 8.5 in the X axis respectively.

The temperature of the cool stream is equal to 14°C. The second inlet was selected to simulate the mouth and nose of a virus-contaminated person in a state of sneezing and coughing. Furthermore, the inlet describing the mouth and nose has dimensions X=5cm and and Y=8 cm.

The person releases a spray of virus-contaminated droplets (C=1, concentration of COVID-19) at a speed of 4.5 m/s. The temperature at this inlet is 40°C. In design 1, there is also a healthy person, whose body temperature is 36.6 °C. Typically, CPU time required to obtain full convergence was 10-14h, depending on the different scenarios simulated and the turbulence model used. Computations were performed on a Windows 7 Server (Intel Xeon 2650 v2 8 core, 2.60 GHz CPU and 32GB of RAM)

4. Results
4.1 Spatial discretization

For the numerical solution, a non-uniform structured grid for each of the two cases is used. The grid is locally refined around the critical area of the two people. Some results of the grid-sensitivity study are given in Fig.3.
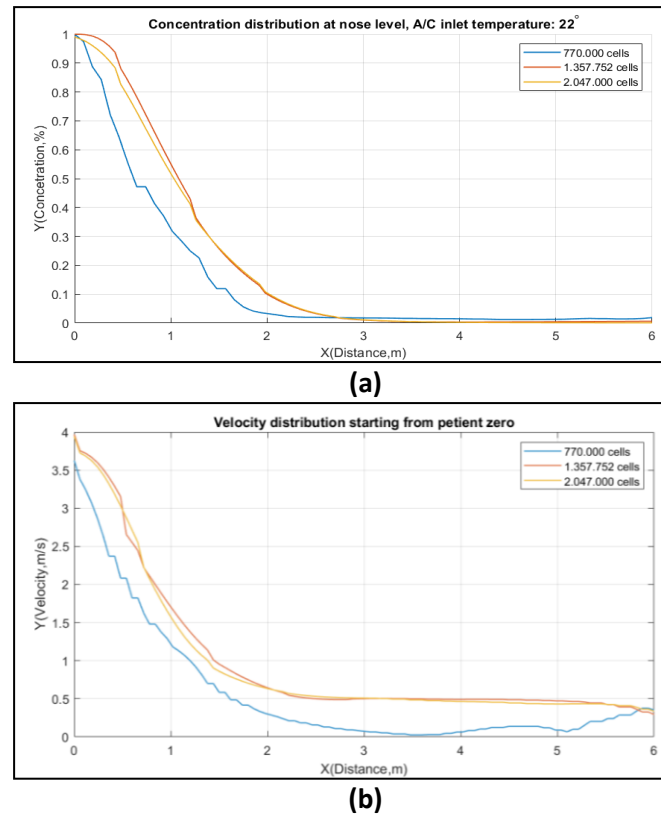

(a)

(b)

Figure 3 - Horizontal distribution of concentration at height z=1.60m between the two human models 770,000 cells blue, 1,357,752 cells red and 2,047,000 cells yellow (a) Concentration (b) Velocity

As is seen in Figure 3, the coarse grid's results for the concentration distribution differ from the results obtained by the other two types of computational grids. The medium and fine grids, however, yield acceptable results.

(a)
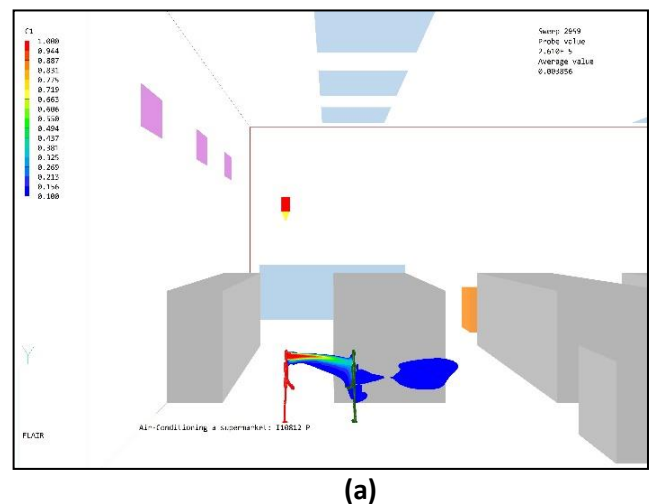
(b)
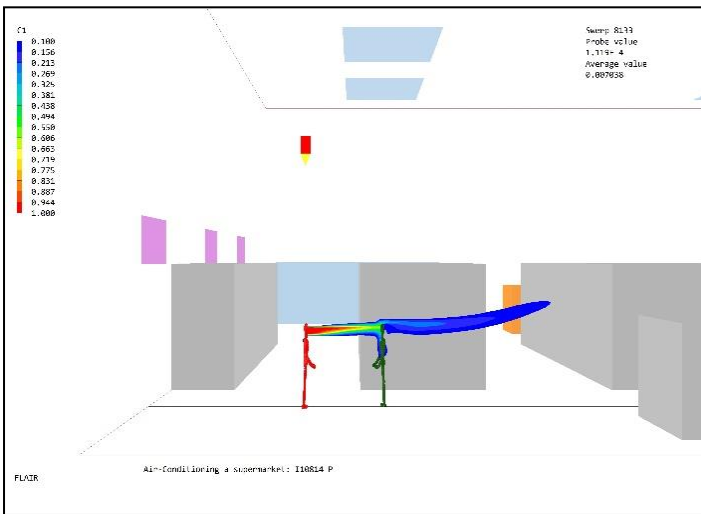
(c)

Figure 4 -- Contour of virus concentration in Y-Plane view, (a) Case 1 A/C units at 8 m height and 14 ℃, (b) Case 2 A/C units at 4 m height and 14 ℃, (c) Case 3 A/C units at 4 m height and 18 ℃

4.2 Calculation of the virus concentration distribution, for different air temperatures

The concentration distribution of the virus was also calculated, for different cases of A/C inlet temperatures, to investigate the effect of the air temperature on the transmission of contaminated particles throughout the space.

More specifically, two cases were examined; in the first one, the air temperature is set equal to 18 ^{o}C, while, in the second, it is set equal to 20 ^{o}C. The distance between the A/C units and the floor remains equal to 4m and the inlet velocity of the air is 0.4 m/s.

In the case of a computational domain with closed windows, the effect is also studied of modifying the A/C inlet velocity on the concentration distribution. First, Figure 5 presents the concentration distribution in the absence of air-conditioning, while, in Figure 6, the concentration distribution for three different air-conditioning inlet velocities is presented. The results were obtained using the k-ω turbulence model.
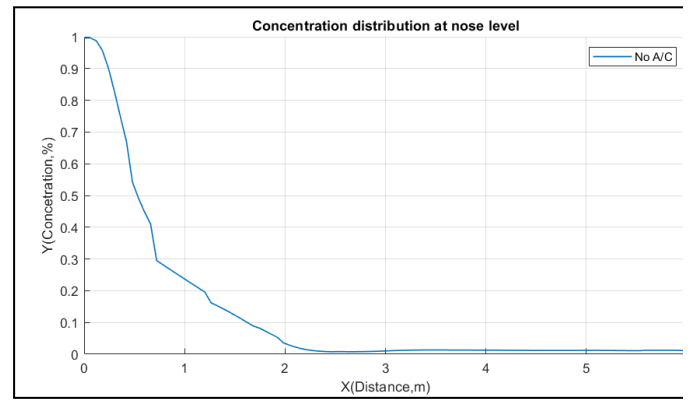

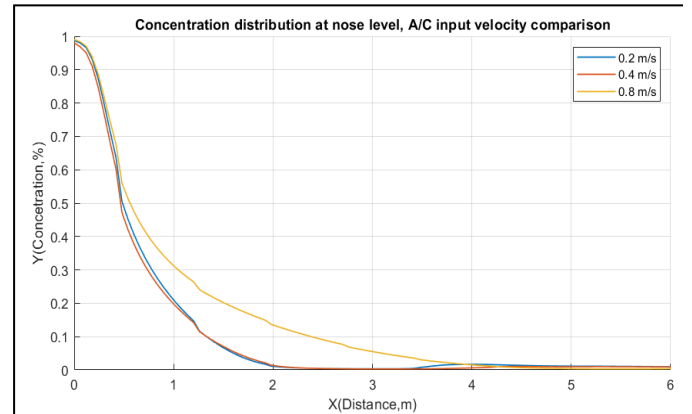**Figure 5 - The virus concentration distribution, with no air-conditioning.**

Figure 6- The virus concentration distribution, for three different air-conditioning inlet velocities, namely 0.2 m/s (mild air-conditioning), 0.4 m/s (moderate air-conditioning) and 0.8 m/s (intense air-conditioning).

As expected, for lower A/C inlet velocities (no air-conditioning), the virus does not get transmitted into a long distance, and its concentration diminishes at a faster rate. However, for an A/C inlet velocity of 0.8 m/s, the virus gets entrained further away, leading to significantly higher concentrations, in the distance range of approximately 0.8 meters to 3.5 meters. This can also be seen in Figures 7 to 9.
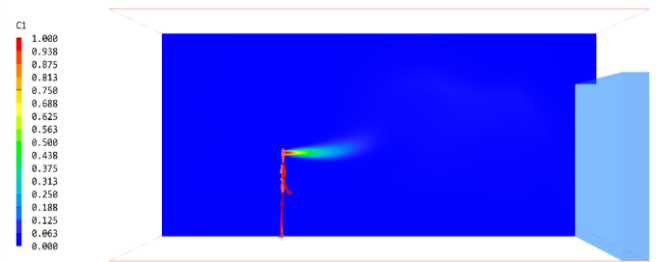

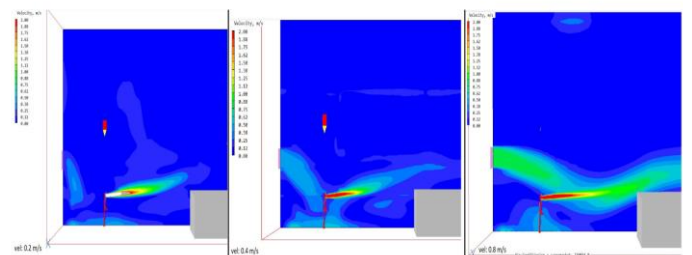**Figure 7 - Virus concentration contours (no air-conditioning).**

Figure 8 - Virus concentration contours (air-conditioning with inlet velocity of 0.2 ,0.4. 0.8 m/s).
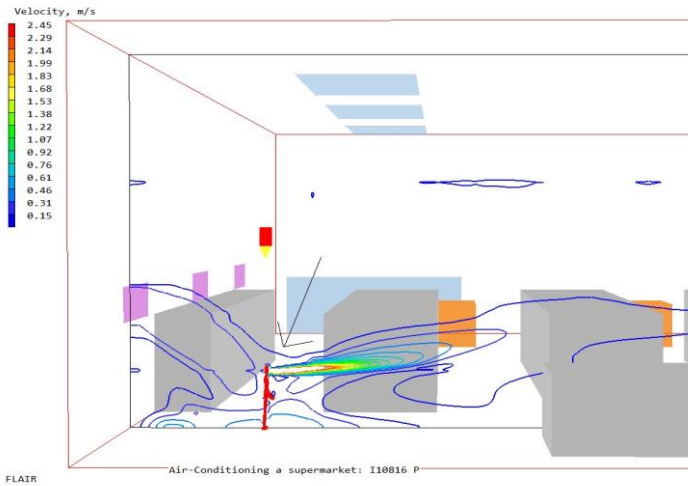
11

Figure 9: Air Streamlines and virus concentration contours (enlarged around the carrier)

From the results, it becomes clear that the virus concentration is quite high, even at a distance of 4m from the contaminated person, at least for two of the three air inlet velocities (approximately 5% for an inlet velocity of 0.2 m/s and approximately 10% for an inlet velocity of 0.8 m/s).

It has been found experimentally that a healthy person has a 17% probability of getting infected at a distance of 1.5 meters from a contaminated person. This probability drops to just 3%, at a distance of 3 meters. If one assumes that the probability of someone getting infected by the virus is proportional to the virus, it follows that this concentration should be equal to 17% at a distance of 1.5m and 3% at a concentration distance of 3 meters.

From the results achieved in this particular case study, it is noticed that the virus concentrations for the three different inlet velocities were calculated as follows:

- Inlet velocity of 0.4 m/s: approximately 19.6% at 1.5 m and 0.7% at 3 m
- Inlet velocity of 0.8 m/s: approximately 30.4% at 1.5 m and 12.8% at 3 m

Thus, an inlet velocity of 0.4 m/s is more favourable for the quicker drop of the virus concentration, while also, seemingly, being in compliance with the experimental observations.

7. Conclusions

Even though the progress in pharmaceuticals and vaccination is remarkable given the short time, their effectiveness can yet be improved. Furthermore, their supply is still limited. Thus, it is still very important to prevent the transmittance of the virus as much as we can. The virus has proven very contagious, and there is strong evidence that it can be transmitted by inhalation of infected saliva in aerosol particles. The creation of these aerosols is from breathing, talking, laughing, coughing, or sneezing.

A big step would be to reduce further the infection due to airborne transmission at the lowest possible level, and at the same time make the presence of people in public places as sustainable as can be. This investigation was conducted to offer an understanding of the airflow patterns in public places. The goal has been carried out to investigate the transmittance distance of the airborne infectious particles. Current social distancing regulations do not consider possible aerodynamics effects such as A/C, windows and doors.

A ventilated internal space without a mask can be seen as a situation for people that must be strongly avoided. In those cases, the virus concentration was higher than 10% until 3m, and it seems fairly safe after 6m. The second design shows that A/C at its higher operation fan speed, enables significantly higher concentration values at the distance between 1 and 3m. Thus, high fan operation speed cannot be recommended. Finally, cases without A/C units have shown less than 10% after 1.65m, which justifies the current regulation that indicates 1.5m as a relatively safe distance.

1. References
[1] Xia Yang, Cuiyun Ou, Hongyu Yang, Li Liu, Tie Song, Min Kang, Hualiang Lin, Jian Hang, Transmission of pathogen-laden expiratory droplets in a coach bus, Journal of Hazardous Materials, Volume 397, 2020, 122609, ISSN 0304-3894
[2] Dhand, Rajiv & Li, Jie. (2020). Coughs and Sneezes: Their Role in Transmission of Respiratory Viral Infections, Including SARS-CoV-2. American Journal of Respiratory and Critical Care Medicine. 202. 10.1164/rccm.202004-1263PP.
[3] van Doremalen N., Bushmaker T., Morris D. H., et al. Aerosol and Surface Stability of SARS-CoV-2 as Compared with SARS-CoV-1. *N. Engl. J. Med.* 2020;382:1564–1567.
 doi: 10.1056/NEJMc2004973.
[4] Reinders Folmer, Christopher & Kuiper, Malouke & Olthuis, Elke & Kooistra, Emmeke & de Bruijn, Anne & Brownlee, Megan & Fine, Adam & Van Rooij, Benjamin. (2020). Compliance in the 1.5 Meter Society: Longitudinal Analysis of Citizens' Adherence to COVID-19 Mitigation Measures in a Representative Sample in the Netherlands in Early April, Early May, and Late May. SSRN Electronic Journal. 10.2139/ssrn.3624959.
[5] Patel, Ashwanee & Dhakar, P.. (2018). CFD Analysis of Air Conditioning in Room Using Ansys Fluent. 10.13140/RG.2.2.13462.50249.
[6] CHAM Ltd, London, UK (2019), PHOENICS (CFD simulation software)
[7] Wilcox, D. C. (1988). Re – assessment of the scale – determining equation for advanced turbulence models. AIAA Journal (Vol. 26, pp. 1299 – 1310). AIAA.

[8] Wilcox, D. C. (2008). Formulation of the k – ω Turbulence Model Revisited. AIAA Journal (Vol. 46, pp. 2823 – 2838). AIAA.

[9] Prandtl, L. (1925). "Z. angew". Math. Mech. 5 (1): 136–139.

[10] Versteeg, H. K., and Malalasekera, W. (2007). An Introduction to Computational Fluid Dynamics: The Finite Volume Method. Pearson Education Limited.

[11] Yakhot, V., Orszag, S.A., Thangam, S., Gatski, T.B. & Speziale, C.G. (1992), "Development of turbulence models for shear flows by a double expansion technique", Physics of Fluids A, Vol. 4, No. 7, pp1510-1520.

[12] Y.S. Chen, S.W. Kim, Computation of turbulent flows using an extended k-∈ turbulence closure model, NASA CR-179204, 1987.
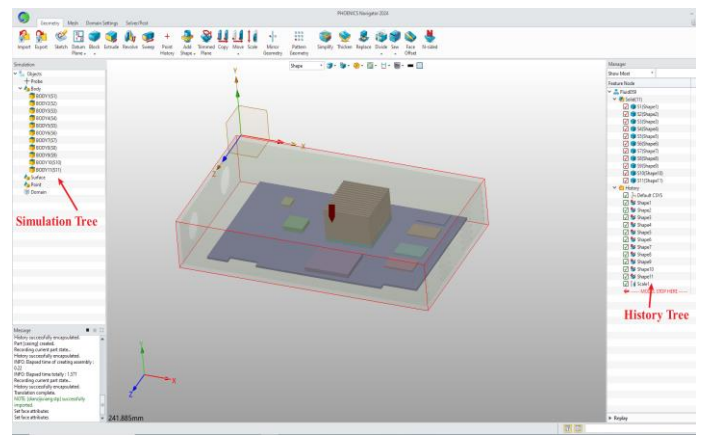
[13] D. Lee, C.L. Yeh, Computation of reacting flame stabilizer flows using a zonal grid method, Numer. Heat Transfer 24 (1993) 173±285.

[14] Stone, H. L. (1968). "Iterative Solution of Implicit Approximations of Multidimensional Partial Differential Equations". SIAM Journal on Numerical Analysis. 5 (3): 530–538. doi:10.1137/0705044. hdl:10338.dmlcz/104038

[15 J C Ludwig (2020) "PHOENICS – Your Gateway to CFD Success Documentation for PHOENICS |TR 006", CHAM Ref: CHAM/TR006, Software version: PHOENICS 2020v1.0

[16] Saad, Yousef & Yeung, M. & Erhel, Jocelyne. (1998). A deflated version of the Conjugate Gradient Algorithm. SIAM Journal on Scientific Computing. 21.

[17] Hamidreza Mortazavy beni, Kamran Hassani, Siamak Khorramymehr, In silico investigation of sneezing in a full real human upper airway using computational fluid dynamics method, Computer Methods and Programs in Biomedicine, Volume 177, 2019, Pages 203-209, ISSN 0169-2607

News Flash: PHOENICS 2024 Released in China Issac Wang ZWSOFT

On March 25, 2024, PHOENICS 2024 was officially released in China. A new CFD pre-processor, based on ZWMeshWorks, named "ZWFluid Simulation: Navigator" (or "PHOENICS Navigator") has been developed. The CFD pre-processing environment has a simple and intuitive graphical user interface, adapted to the core-solver module PHOENICS, and provides a fully Chinese user environment.

The main interface of Navigator consists of a simulation tree, a history tree, a view area, and a Ribbon bar, with the Ribbon bar divided into four major parts: Geometry, Mesh, Domain Settings, and Solver/Post. The latter option includes Solve, Parallel Settings and the button to start the Post-Processor.

In the simulation tree, we can store by category, different types of objects such as Body, Surfaces, and monitoring points. If we import geometric models in different formats, the three-dimensional shape of the model will be put in Bodies, and the two-dimensional shape in Surfaces. Similarly, if we create an object in Navigator, we divide the object type into two categories.

The first is that the Blockage, Angled in, Angled out, Foliage, Sun and Wind objects will be hung under the, Body node after creation, and the other category is that after the Fan, Inlet, Outlet, Plate and Thin Plate objects will be hung under the Surface nodes after construction. Double-clicking on an object in the simulation tree allows for operations like display/hide/delete and property editing.
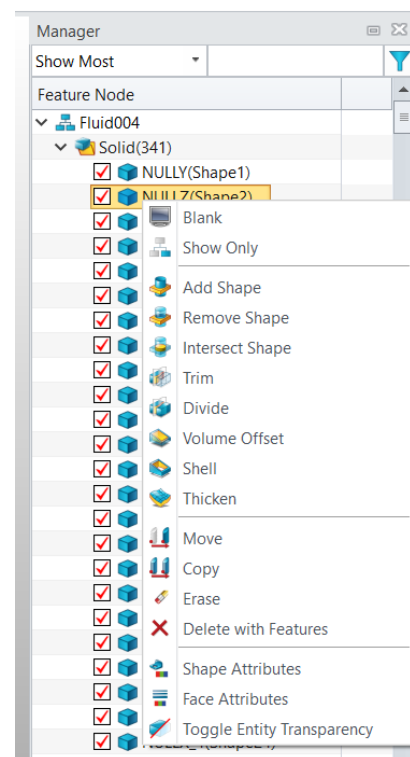
In the history tree, you can perform historical rollback for geometric editing, and you can also perform some editing on entities and modify editing history. Set down below is a detailed illustration of the history tree.
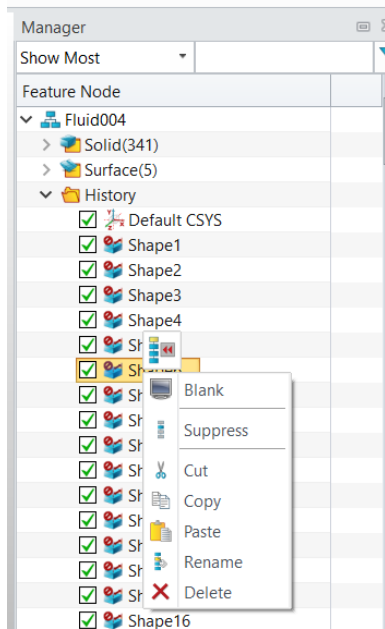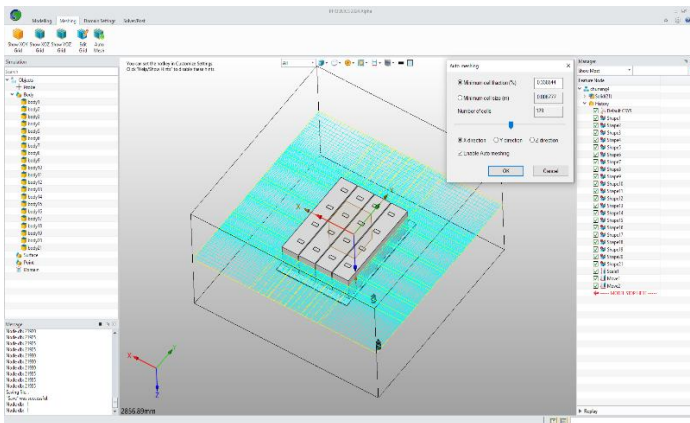
In the grid module, we can display the grids of different planes both separately and simultaneously.

There are two methods of editing the grid: automatic and manual.

On starting PHOENICS 2024 you can select entering either the Navigator for pre-processing, or the classic VR interface. Both operating environments support switching between Chinese and English languages.

We have completed the integration of PHOENICS into the ZWMeshWorks platform, incorporating the geometric editing capabilities of ZW3D. In this phase, the platform still calls the PHOENICS VR panels to complete the pre-processing, creates the Q1 file, generates EARDAT through SATELLITE, and transfers the data to the solver for calculation. Finally, post-processing is done in the VR-Viewer.
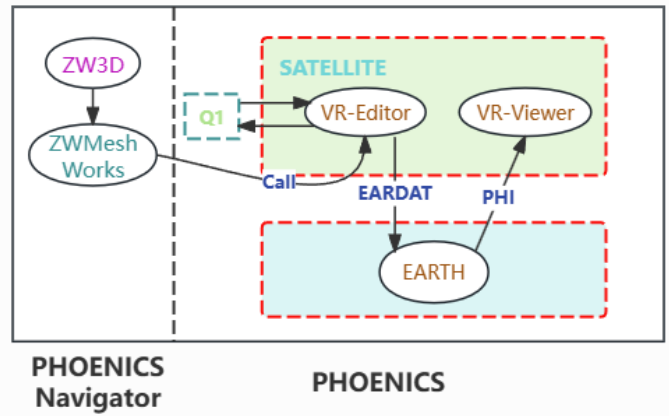
We hope that this new upgrade to the Graphical User Interface of PHOENICS will be well received and supported by both new and old customers! We invite everyone to use the PHOENICS Navigator and provide us with valuable feedback and suggestions, so that we can improve PHOENICS together.

A Review of Some Recent PHOENICS Publications
Michael R. Malin, CHAM

1. Introduction
PHOENICS was the first general-purpose CFD code to appear on the market in 1981, and therefore it has acquired a long history of usage across a very diverse range of applications. Since the inaugural PHOENICS publication of Professor Brian Spalding [1], the intervening four and a half decades have seen an expansive number of publications making use of this code. In this article, the attention is focussed on describing briefly a small sample of PHOENICS-based articles published in recent times. In the ensuing paragraphs, the following applications are described: the simulation of heat-transfer technology in tubing; the windborne deposition of marine salts on buildings near a river estuary; and the performance of a phase-change-material battery in the climate tower of a building.

2. Enhanced Turbulent Heat Transfer in Tubes
The use of **helical coiled-wire** and **twisted-tape inserts** in circular tubes is common in industry as a reliable method for enhancing heat transfer by inducing a swirling motion upon the axial-directed core flow. These inserts find applications in heat exchangers, oil-cooling equipment, preheaters, fire boilers and the divertors of fusion reactors.

In a joint collaboration, and for flow conditions typical of a divertor, **HATA Research Institute** and **Kobe University** in **Japan** [2] used PHOENICS to predict the heat-transfer performance and pressure drop for the flow of water in tubes with inserts.

The geometry of the insert was created in SolidWorks, and then imported into PHOENICS. The PARSOL cut-cell solver was used to capture the insert geometry on the background cylindrical-polar mesh; and the turbulence was modelled by means of the high Reynolds-number (Re) form of the Chen-Kim variant of the k-ε model.

Converged solutions were obtained by time marching to steady-state conditions. Experimental and numerical results were reported, both with and without inserts, in the Re range of 20,000 to 100,000, for a tube of 6mm diameter (d) tube and length 104d, with a heated section of 10d, starting some 55d downstream of the inlet.

PHOENICS predictions of the pressure drop were within 5% of measurements, whereas predicted rises in water temperature showed deviations ranging from 0 to 20%. The results were also presented in terms of the Fanning friction factor and Nusselt number vs Reynolds number.

3. Marine-Aerosol Deposition in an Estuary
The airborne transport of marine chloride-salt aerosols in coastal areas can result in surface deposition on buildings and other structures. This type of exposure promotes weathering and decay processes, which can damage not only the surfaces of buildings, but also their structural integrity.

PHOENICS was used by the **South China University of Technology** [3] to investigate the deposition of chloride salts on building surfaces in the Zhujiang River Estuary. Specifically, the wind fields of NanHeng Village and Zhujiang International Apartment were simulated to explore the effects of building-related factors on chloride-salt deposition.

The main findings were: narrower spacings between buildings promoted greater deposition; surface deposition correlated linearly with offshore distances in the range 500–1500m; and, under unobstructed conditions, surface deposition correlated positively with building elevations in the 10–100m range.

4. Phase-Change Materials (PCMs) in Buildings
PCMs are substances with a high latent heat. This is stored during phase transition, when thermal energy is absorbed and released at essentially constant temperature during the melting and solidification phases. This feature can be used to lower the energy consumed by conventional heating and cooling systems, by reducing peak loads. Consequently, PCMs have been used extensively in the buildings for many years. In particular, they have been exploited to realise the management of interior temperature against external weather and temperature variations.

In a recent study, **Delft University of Technology** in the **Netherlands** [4] investigated, both experimentally and theoretically, the performance of a PCM battery installed in the climate-control tower of a building.

The climate-control system comprised a heat-recovery unit, a battery of PCM plates which buffer any fluctuations in the supply-air temperature, and an auxiliary heat pump. For the theoretical investigation, transient CFD simulations were performed using PHOENICS; and system control and optimization, a simplified lumped-parameter model was implemented in MATLAB . Technical support was provided by **CHAM** on the CFD modelling of the PCM melting and solidification process.

A transient, three-dimensional CFD model was developed to simulate the flow and heat transfer within the PCM battery. The liquid and solid regions of this battery were housed within solid casings, and were subject to conjugate heat transfer with the air flow in the adjacent channels. The PCMs experienced melting and solidification processes, with natural convection in the melt. Phase transition was modelled using an enthalpy-porosity formulation, but by means of an effective specific heat capacity, rather than a latent-heat source term. The InForm facility of PHOENICS was used to implement this phase-change model.

The transient performance of the PCM battery through heating and cooling was evaluated by using a steady air-inflow rate at three different inlet velocities with a constant inlet temperature. Reasonable agreement was reported between the measured and predicted temperature behaviour, with a maximum variance of 10%.

5. Concluding remarks
This brief review gives some insight into PHOENICS usage for applications related to the nuclear, environmental and buildings industries. In future issues of the Newsletter, similar reviews will be conducted to inform readers of other PHOENICS-based publications originating from Academia and Industry.

6. References
1. D.B. Spalding, *A general-purpose computer program for multi-dimensional one- and two-phase flow*. Mathematics and Computers in Simulation, 23, 267–276, (1981).
2. K. Hata, M. Shibahara, *Helically-coiled-wire-induced swirl flow heat transfer and pressure drop in a circular tube under velocities controlled*, Int. J of Heat & Mass Transfer 204, 123849, (2023).
3. L.Xiang , Q.Meng , P.Ren, *Effects of environmental and architectural factors on chloride-salt deposition on coastal building surfaces in the Zhujiang River Estuary*, Building & Environment 242, 110554, (2023).
4. P. van den Engel, M.R.Malin, N.K.Venkatesh and L.A. de Araujo Passos, *Performance of a Phase Change Material Battery in a Transparent Building*, Fluid Dynamics & Materials Processing, Vol.19, No.3, (2023).

News from CHAM:

On the 17th of April Truman Du, CEO of ZWSOFT paid a visit to CHAM for a meeting with CHAM Management and then took CHAM staff out for a meal along with members of the Guangzhou CFD Team.

Contact Us:

CHAM's highly skilled, and helpful, technical team can assist in solving your CFD problems via proven, cost-effective, and reliable, CFD software solutions, training, technical support and consulting services. If YOU have a CFD problem why not get in touch to see how WE can help with the solution?

Please call on +44 (20) 89477651, email sales@cham.co.uk or check our website www.cham.co.uk. For PHOENICS on the Cloud (PHOENICS-OTC) call us or contact phoenics.cloud@cham.co.uk

See us on social media sites shown below: